remote sensing

MDPI

Review

Using CORONA Imagery to Study Land Use and Land Cover Change—A Review of Applications

Mahsa Shahbandeh [1,2,*], Dominik Kaim [2] and Jacek Kozak [2]

[1] Doctoral School of Exact and Natural Sciences, Jagiellonian University, Łojasiewicza 11, 30-348 Krakow, Poland
[2] Institute of Geography and Spatial Management, Faculty of Geography and Geology, Jagiellonian University, Gronostajowa 7, 30-387 Krakow, Poland
* Correspondence: m.shahbandeh@doctoral.uj.edu.pl; Tel.: +48-12-664-5302

Abstract: CORONA spy satellites offer high spatial resolution imagery acquired in the 1960s and early 1970s and declassified in 1995, and they have been used in various scientific fields, such as archaeology, geomorphology, geology, and land change research. The images are panchromatic but contain many details of objects on the land surface due to their high spatial resolution. This systematic review aims to study the use of CORONA imagery in land use and land cover change (LULC) research. Based on a set of queries conducted on the SCOPUS database, we identified and examined 54 research papers using such data in their study of LULC. Our analysis considered case-study area distributions, LULC classes and LULC changes, as well as the methods and types of geospatial data used alongside CORONA data. While the use of CORONA images has increased over time, their potential has not been fully explored due to difficulties in processing CORONA images. In most cases, study areas are small and below 5000 km^2 because of the reported drawbacks related to data acquisition frequency, data quality and analysis. While CORONA imagery allows analyzing built-up areas, infrastructure and individual buildings due to its high spatial resolution and initial mission design, in LULC studies, researchers use the data mostly to study forests. In most case studies, CORONA imagery was used to extend the study period into the 1960s, with only some examples of using CORONA alongside older historical data. Our analysis proves that in order to detect LULC changes, CORONA can be compared with various contemporary geospatial data, particularly high and very high-resolution satellite imagery, as well as aerial imagery.

Keywords: CORONA imagery; declassified spy satellite; high-resolution images; land use and land cover change

Citation: Shahbandeh, M.; Kaim, D.; Kozak, J. Using CORONA Imagery to Study Land Use and Land Cover Change—A Review of Applications. *Remote Sens.* **2023**, *15*, 2793. https://doi.org/10.3390/rs15112793

Academic Editor: Georgios Mallinis

Received: 7 February 2023
Revised: 23 May 2023
Accepted: 25 May 2023
Published: 27 May 2023

1. Introduction

The government of the United States of America (U.S.) started the space-borne photography CORONA program in the 1950s, with the first successful image acquisition in August 1960 [1,2]. Lasting until May 1972, CORONA was the first high-resolution satellite imagery [3] dedicated to military intelligence purposes. The mission was to monitor Soviet missile strength [4] and Chinese nuclear programs [5], but it had global spatial coverage, particularly in Eastern Europe and Asia [6]. The CORONA program consisted of satellites launched by Thor-Agena rockets [5,7] that were equipped with various panoramic camera models (referred to as Keyhole, KH), providing a black and white 70 mm film [5], with KH-4B having the best spatial resolution [8,9] (Table 1). Cameras of the satellites of the CORONA program were calibrated by concrete targets on the ground in Arizona [10]. After 12 years of service, the mission was replaced by HEXAGON, a Central Intelligence Agency (CIA) program [11]. While the CORONA name typically refers to satellites using KH-1 to KH-4B cameras, two other camera systems, ARGON (KH-5) and LANYARD (KH-6), operating in 1961–1964 and 1963, respectively, were also part of the CORONA program [1,9].

Table 1. CORONA satellites and cameras details [12,13].

Satellite and Camera	Time Period	Resolution
KH-1	1959–1960	7.5 m
KH-2	1960–1961	7.5 m
KH-3	1961–1962	7.5 m
KH-4	1962–1963	7.5 m
KH-4A	1964–1969	2.75 m
KH-4B	1967–1972	1.8 m

The CORONA images were declassified in 1995 by Executive Order 12951 because the program was no longer considered to be crucial to national security [14]. The primary archive of the imagery—analog photographic products containing film negatives and photo prints that include 800,000 photographs—is stored by the National Archives and Records Administration (NARA) at the National Archives in College Park, Maryland [14–16]. Following the 1995 declassification of military imagery, the dataset was converted into digital form and made available by the United States Geological Survey (USGS), together with imagery of the follow-up missions in 1995 (Declass 1 dataset), 2002 (Declass 2 dataset) and 2011 (Declass 3 dataset) [14,17,18].

A single CORONA image is a narrow strip, with size depending on the camera type, and it is approximately 20 km wide and 200 km long [9,16,18,19]. Unprocessed CORONA images have severe spatial distortions [20] and contain limited spectral information due to 8-bit panchromatic (single band) image depths [21]. As a result of a dual-angle system of two panchromatic cameras at 15 degrees off-nadir in KH-4, KH-4A and KH-4B systems, it allows also producing a digital elevation model [16,22].

Due to the availability of CORONA imagery since 1995, many researchers used the data to study various environmental processes [23], for instance, past land cover in the Caucasus Mountains [24], forest habitat fragmentation in the Bucegi Mountains, Romania [25], and post-agricultural forest succession in the Carpathian mountains [26]. In many studies, CORONA images were used jointly with other geospatial data to assess changes in land use and land cover (LULC) since the 1960s [27,28], with several studies reporting substantial difficulties when processing the data [6,29,30]. Although CORONA images were widely used in many research fields and the number of studies is increasing, a comprehensive assessment of CORONA imagery applications in studying LULC changes is still missing. However, previous studies that reviewed CORONA imagery were mainly related to technical issues, such as camera construction, imaging and algorithms [16,31]. In this review paper, we therefore aimed to find out how CORONA imagery was used so far in LULC change studies, particularly looking at how they compare to other historical or contemporary geospatial data and how they were analyzed to assess the LULC change. This is important as a broad spectrum of current spatial datasets differs substantially in nature from old spatial data that may offer high potential for LULC studies.

2. Methods

In our research, we followed a typical research design of the systematic review [32,33], starting first with querying a database of scientific papers, defining criteria of research paper selection, selecting research papers for analyses and examining the content of research papers according to a structured set of questions [34].

For our analysis, we used the SCOPUS database (www.scopus.com, accessed on 1 April 2023), a general database of research publications that has been used in various review papers [34,35]. To select papers in which CORONA data could possibly be analyzed, we searched article titles, abstracts and keywords by using the following set of expressions connected by logical OR:

- declassified corona data
- "corona image"
- corona spy satellite

- declassified spy satellite
- "corona images"
- "corona imagery"

To build the query, we used quotation marks in case *Corona* was used jointly with *image*, *imagery* or *images*, as our initial trials showed that a simple phrase such as *corona image* (or *corona imagery* or *corona images*) provided a high number of papers related, e.g., to astronomy or medical sciences (for instance, COVID-19-related papers). The search was carried out by the end of 2022, and we set no restrictions for the publication year.

The final set of selected publications was initially screened first to remove papers that did not use CORONA imagery and that were accidentally selected from the SCOPUS database. Next, we examined the remaining papers using CORONA data and identified papers with a focus on LULC studies. For the LULC studies, we used a set of research questions to analyze the content of publications in the context of LULC and LULC changes. These questions were grouped into spatial, temporal and thematic aspects of the selected studies:

1. Spatial aspects
    - 1.1. In which regions and countries CORONA images were used?
    - 1.2. What was the size of the study area?
    - 1.3. How did CORONA images cover the study area (entire study area–wall-to-wall mapping or a part of the study area using pre-defined sampling)?
2. Thematic aspects
    - 2.1. What LULC categories were studied using CORONA images?
    - 2.2. Which methods of LULC identification, interpretation and analysis were applied for CORONA images?
3. Temporal aspects
    - 3.1. Was the LULC analysis a single moment (related to the 1960s-1970s, using only CORONA images and other geospatial data for this time period) or was it multitemporal?
    - 3.2. If it is multitemporal, what time period was analyzed in the study?
    - 3.3. If it is multitemporal, what geospatial data were analyzed alongside CORONA images?

For question 2.1, we used 7 basic LULC categories from global land cover mappings [36] (forest, grassland, cropland, built-up, bare land and sparse vegetation; wetland and water; and snow and ice). For question 2.2, referring to methods used for CORONA imagery analyses, we were interested primarily in the division of manual versus automated image interpretation, specifying classification approaches for the latter. For question 3.3, regarding geospatial data, we grouped the data used in various studies into 7 classes: topographic maps; low and medium spatial resolution satellite images (pixel size > 100 m; LR images); high-resolution satellite images (pixel size 10–100 m, HR images); very high-resolution satellite and aerial images (pixel size < 10 m; VHR images); LULC thematic maps; field measurements; and others.

3. Results

3.1. Database Query

The query expression returned 154 items in total: 147 were research articles, 3 were review papers and 4 were book chapters published since 1995. From the initial set of 154 research publications, we rejected 53 publications: 38 were not relevant to CORONA imagery (e.g., related to research domains such as nanotechnology or astronomy), 8 papers were in languages other than English (two Korean, five Chinese and one Italian), 4 were book chapters, and 3 were review papers. Book chapters and review papers presented overviews or technical aspects of the CORONA program mostly in the context of archaeological applications. In the remaining set of 101 research articles, we identified 54 papers

dealing with LULC for further analyses (full list see Appendix A). The other 47 papers dealt with digital elevation modeling and geomorphology (22), archaeological applications (19) or technical aspects of the CORONA program (6) (Figure 1). Further on, we only analyze and discuss the set of 54 LULC papers.

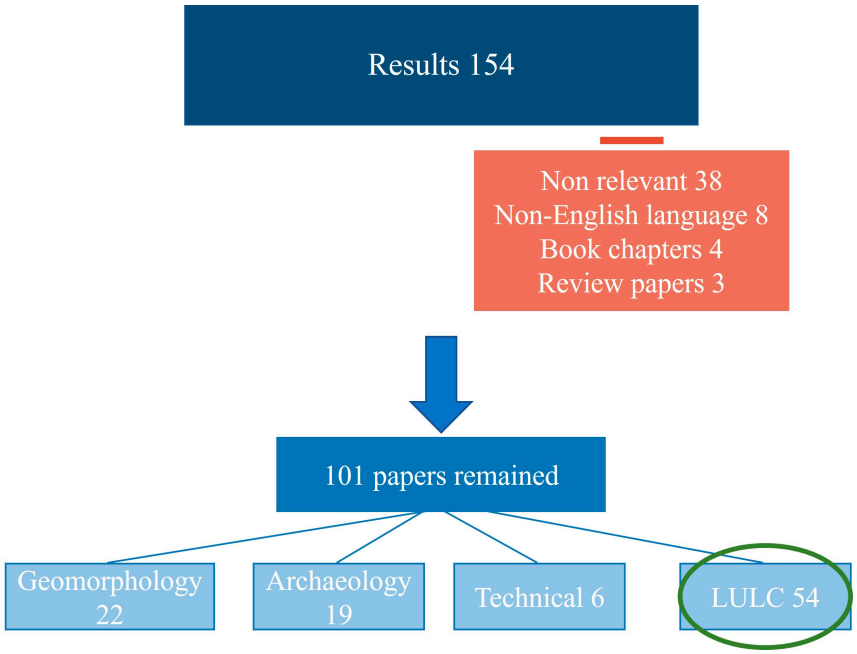

Figure 1. SCOPUS query results and selection of the subset of LULC-related papers.

With respect to the papers examined in this study, 54 LULC-relevant papers were published in 37 journals, with only 2 journals publishing more than 2 papers: *Remote Sensing* (11 papers) and the *International Journal of Remote Sensing* (4). Publication years varied, starting in 2000 (Figure 2). Recent years (2020, 9 papers; 2021, 10 papers; 2022, 6 papers; Figure 2) show increasing interest in using CORONA imagery to study LULC compared to the first two decades after declassifying CORONA data in 1995.

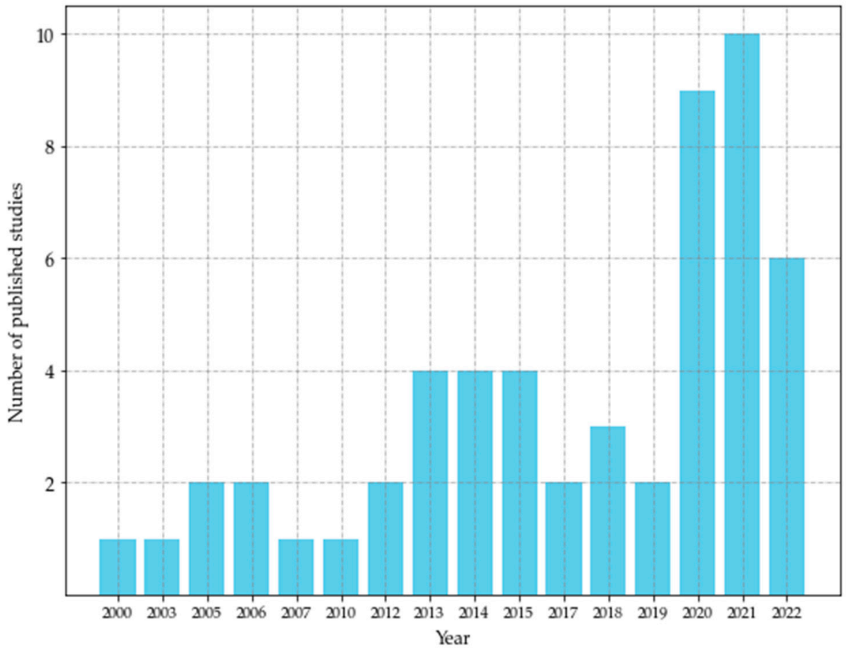

Figure 2. Number of LULC-relevant studies using CORONA imagery published per year.

3.2. LULC Studies with CORONA Imagery

3.2.1. Spatial Aspects

The case studies were located in 36 countries (Figure 3, Appendix A). Most studies were carried out in Russia, China, Central and Eastern Europe, the Middle East and Western Africa. However, there are substantial gaps with respect to country-level geographical coverage, for instance, in Western Europe.

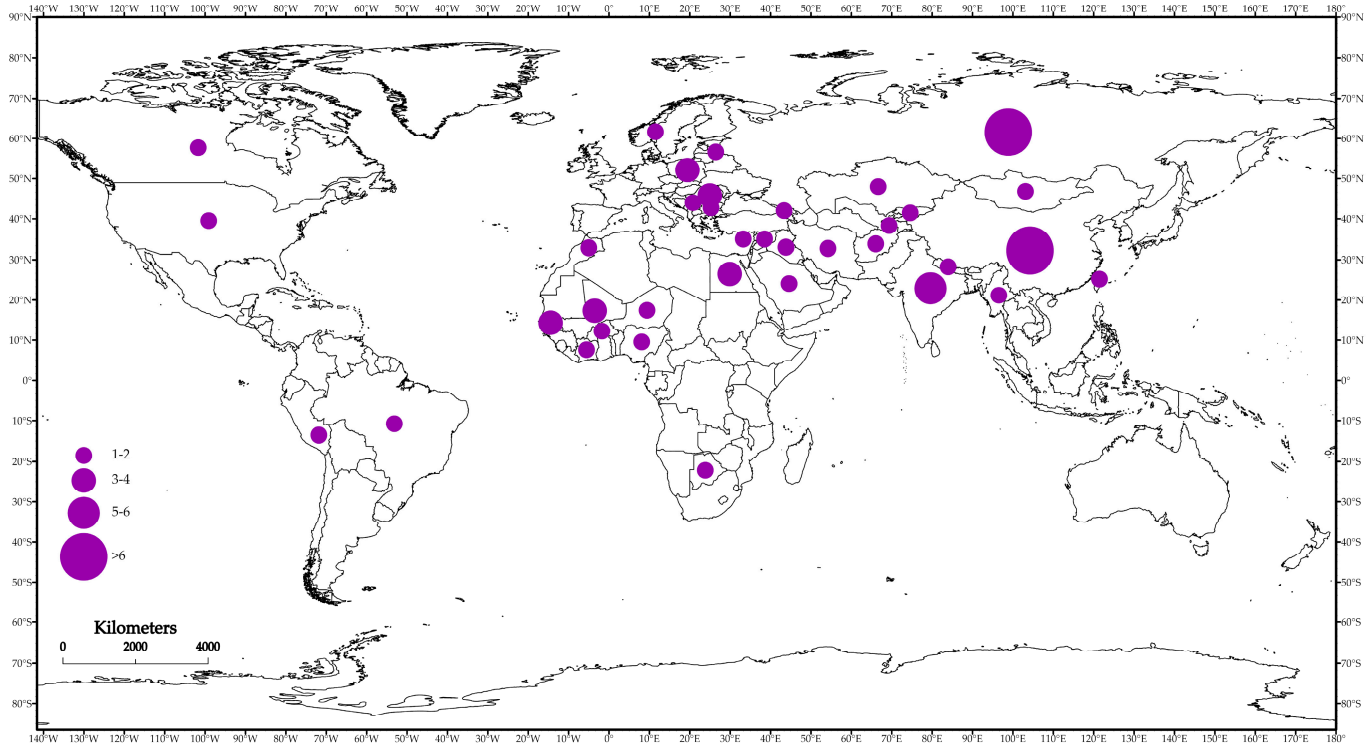

Figure 3. LULC case studies with CORONA imagery: country distribution.

The size of the study area varied from a small area of around 2 km^2 [37] to a large area of approximately 484,000 km^2 [30], and in one case, the size was even more than 1 million km^2 [38]. In 34 case studies, CORONA imagery covered the entire study area (wall-to-wall mapping) while 19 studies used CORONA to investigate a part of the study area using a pre-defined sampling strategy. In one paper, a combined approach of a wall-to-wall timberline mapping and analysis of forest cover based on 43 sample small plots was used [39]. For 22 papers, the area of case study sites was not explicitly given, and we estimated the areas based on maps published in the papers.

A wall-to-wall mapping of an entire study area using CORONA imagery was almost three times more common than carrying out sampling when the size of the case study area was less than 5000 km^2. On the contrary, for study areas exceeding 5000 km^2, a typical approach was to sample part of the study area for analysis (Figure 4).

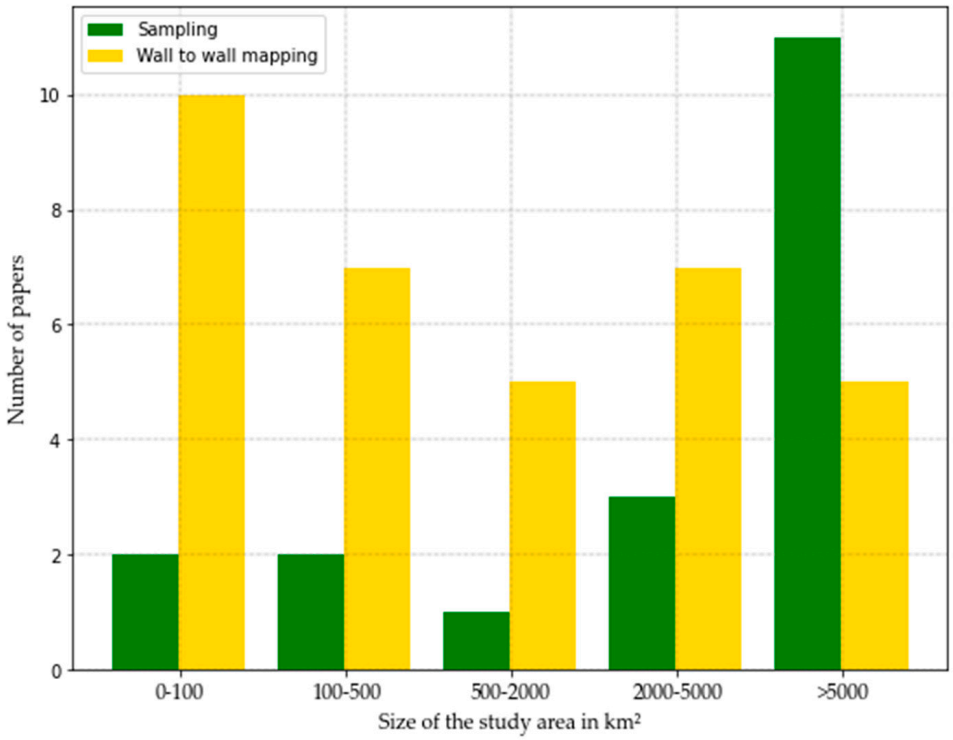

Figure 4. Size of the study area in relation to CORONA imagery coverage.

3.2.2. Thematic Aspects

Most studies considered several LULC categories simultaneously, while 24 out of 54 papers focused solely on one single LULC category. Forests were the most frequently studied LULC category, followed by wetlands and water bodies, bare land and sparse vegetation land cover classes (Figure 5, Appendix A).

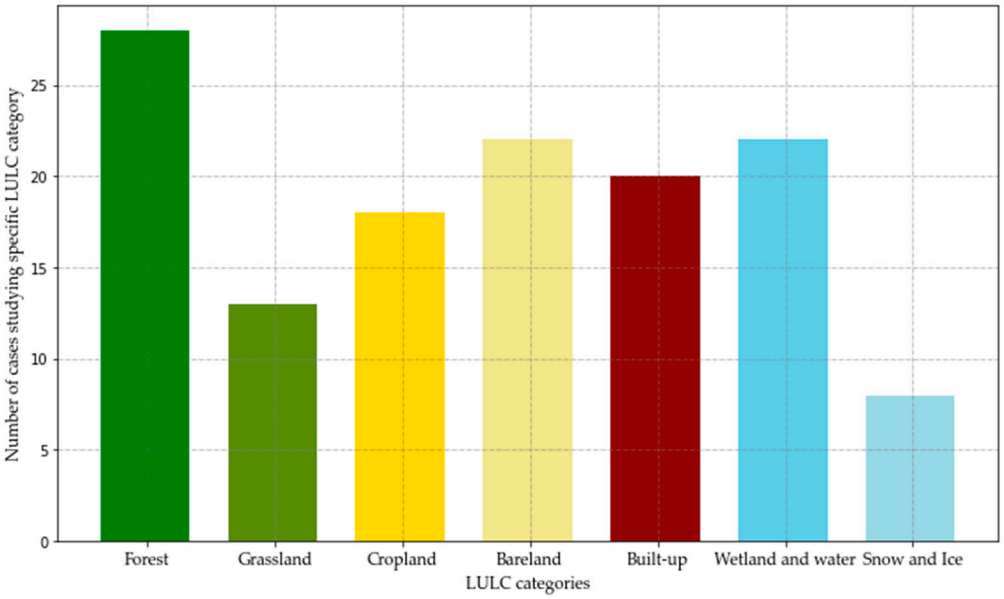

Figure 5. LULC categories studied in the analyzed papers.

With respect to the studies reviewed here, 35 studies used manual interpretation (on-screen vectorization) and 13 studies used automated classification, while 6 studies combined manual interpretation and automated classification to extract LULC information from CORONA imagery (Appendix A). With automated approaches, forest and cropland

were preferred over other LULC categories. We identified nine studies that used automated classification to map the entire study area (wall-to-wall mapping). The study area sizes in this subset of studies ranged from 8 km^2 [40] to 44,957 km^2 [41]. Among automated approaches, object-based image analysis (OBIA) or various classification approaches using the textural features of CORONA imagery were applied (11 out of 13 studies).

3.2.3. Temporal Aspects

Five studies were confined to single-moment analysis of LULC at the moment of CORONA imagery acquisition (Appendix A). These studies were highly varied and included forest cover mappings carried out in the 1960s–1970s [42], the use of panchromatic images to generate enhanced multi-layer products [43], and testing land cover classification methods [42,44,45].

In total, 49 papers represented a multitemporal approach (Appendix A), with CORONA imagery being one of the datasets used in the time series spanning the entire study period. In 42 studies, the beginning of the study period took place in the 1960s or 1970s, with CORONA imagery being the oldest dataset used to assess LULC at the beginning of the study period. Seven studies analyzed LULC changes before the launch of the CORONA program using older data than CORONA, for instance, archival maps, historical or archival records and older aerial photographs, with CORONA imagery being an intermediate dataset of the entire time series. The study period extended in most cases into the 21st century (46 studies), with only three studies considering LULC changes solely in the 20th century (Figure 6).

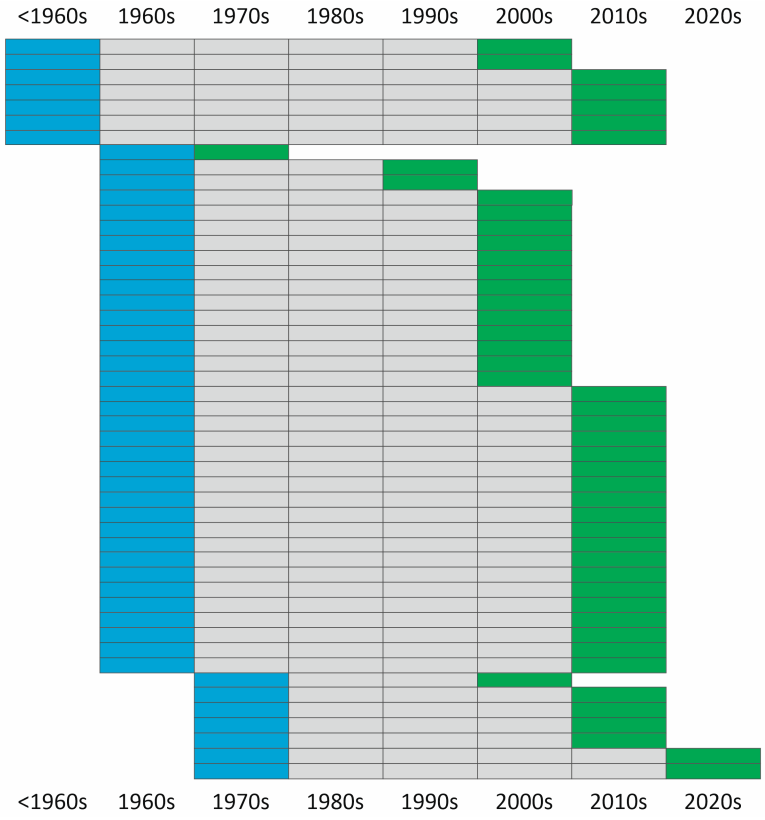

Figure 6. Time periods in the analyzed case studies. Each row represents one case study; blue color indicates the beginning, and green indicates the end of the study period.

Multitemporal studies used various geospatial data to detect LULC and its changes by comparing them with CORONA imagery (Figure 7). The dominant type of data used in multitemporal studies were very high-resolution images of various observation programs,

platforms and data archives. However, among various types of imagery, Landsat was the most frequently used dataset that was analyzed jointly with CORONA (25 studies).

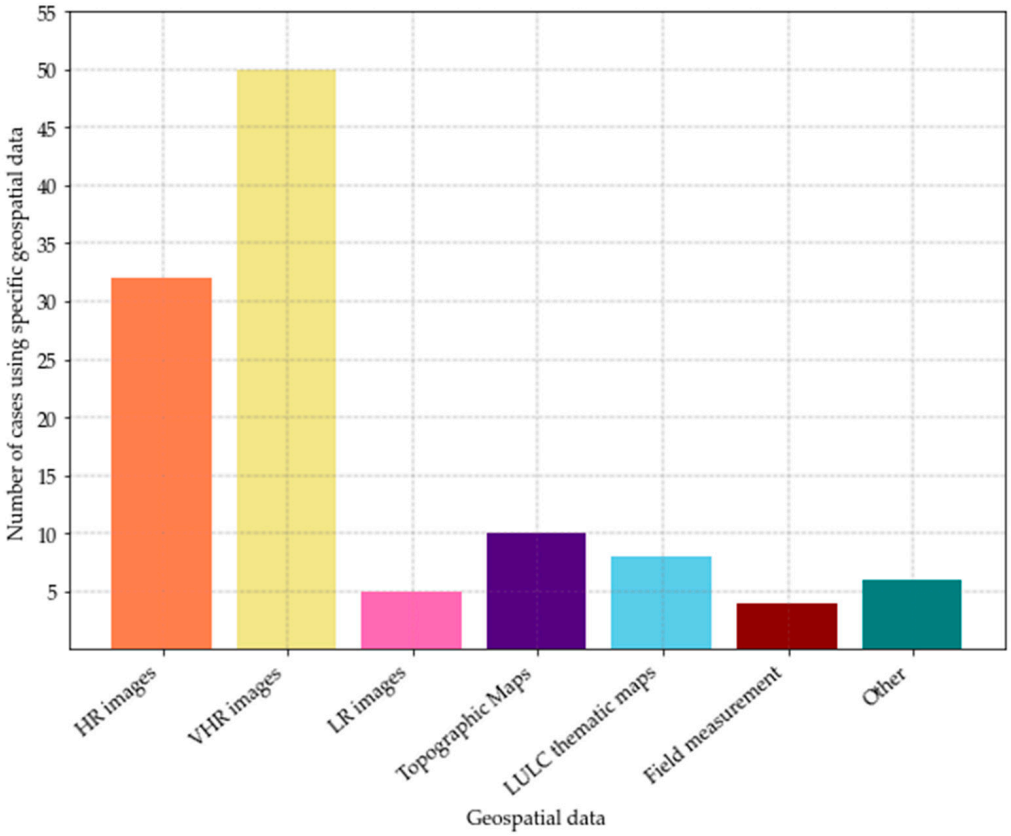

Figure 7. Various data types used with CORONA imagery to study LULC. HR: High-resolution images; VHR: very high-resolution images; LR: low-resolution images.

Multitemporal studies focused on forest cover changes (deforestation, forest expansion and degradation of dryland forests), urban expansion, changes in water bodies and glacier extents. To study and detect forest cover changes, high-resolution imagery, such as Sentinel-2, and Landsat as well as LULC thematic maps were mainly used [28,46]. Only a small number of studies employed low-resolution satellite imagery; e.g., a moderate-resolution imaging spectrometer (MODIS) was used to analyze changes in snow cover and ice extent [47]. One interesting feature of using CORONA imagery is that the very high-resolution imagery of HEXAGON and GAMBIT (the follow-ups of the CORONA mission) was jointly used with CORONA to study changes in urban areas [5].

4. Discussion

Following the declassification of imagery acquired during the CORONA and subsequent missions in 1995, LULC studies using spy satellite image data started to increase in numbers, reaching a total of 54 papers by the end of 2022, with case studies located in different countries and covering all continents except for Australia and Antarctica; however, one of the early research papers published in 1998 used CORONA imagery in a glaciological study of the Ross Ice Shelf [48]. Quite interestingly, some studies that had been included in the preliminary set relevant to the LULC analysis had to be removed after a detailed inspection of the papers, as it revealed that they were using imagery acquired in the CORONA program's follow-up missions (HEXAGON) and not the imagery of the CORONA program [49,50].

As the mission of CORONA was to provide images, especially of the Soviet Union and China [51], these two countries were featured in most LULC studies in which CORONA

data were used. Our results showed that except for present-day Russia and China, CORONA imagery was also commonly used in India and Nepal; the Middle East (Iraq, Iran and Syria); Northern and Western Africa (Egypt, Mali and Senegal); and Central and Eastern Europe (Poland and Romania) [26,28,30,42–44,52–58]. Some of these countries (e.g., Poland and Romania) have good coverage of CORONA imagery due to the goals of the program and the importance of the countries during the Cold War era [59–61]. One of the reasons that probably pushed researchers to use CORONA in several countries listed here is the poor availability of comparable aerial data that are not easily accessible via online archives, although they exist [5]: for instance, aerial data for Poland acquired in the 1950s or the 1960s. At the end of 2022, we could not find any LULC studies using CORONA imagery in various countries that potentially provide good coverage of these data (post-Soviet countries, such as, e.g., Ukraine or Belarus), suggesting that CORONA data have not been fully explored within the LULC context yet. This is changing, however, with new studies published for various post-Soviet areas, such as the Caucasus Mountains [24].

We noted two strategies for using CORONA imagery to study LULC and its changes in the selected case study areas. In approximately two-thirds of the studies, with a case study area that is typically less than 5000 km^2, researchers attempted to find and later analyze full CORONA coverage for the entire study area. The other papers, typically with case study areas exceeding 5000 km^2, used CORONA data only for selected fragments of their study area. The reason for the focus on small case study areas or fragments of large study areas is related to the size of a single CORONA strip (depending on the camera, approximately 4000 km^2) and its width (approximately 20 km), which pose various difficulties related to geo-rectifying the strips in larger study areas [22]. Spatial distortions in CORONA images are difficult to reduce and may result in significant errors when overlaying and comparing them with contemporary very high-resolution satellite and aerial images [44,62,63]. Our findings confirm that spatial distortions are a major problem when using CORONA imagery, as the case studies mostly use the manual or semi-automated rectification and georeferencing of CORONA data. While no fully automated approach for this processing step was provided, Nita et al. [42] developed a CORONA imagery orthorectification method by relying on the structure from motion technology and were able to efficiently process more than 200 CORONA strips for a study area exceeding 200,000 km^2. Mean absolute errors were less than 4 m in flat areas but increased to 10 m in hilly areas and over 20 m in mountainous areas [42]. Song et al. [6] used the scale-invariant feature transform to match CORONA imagery to Landsat data and received errors close to one Landsat MSS pixel. In other studies, the reported root mean square errors were around 10 m [26,29,62].

Spatial distortions of CORONA images also contribute to difficulties in image mosaicking. In addition, receiving a seamless coverage of CORONA imagery for large areas is extremely demanding due to radiometric differences, acquisition frequency and cloud-free image availability, forcing researchers to analyze CORONA imagery rather than on a one-to-one basis [64]. Leempoel et al. [65] and Gurjar and Tare [66] in their research mentioned that these specific problems in using and processing declassified CORONA images are quite challenging. A frequent approach, therefore, is to use CORONA imagery as a sample that covers only a part of the larger area, focusing, e.g., on specific objects or locations of interest. For instance, Marzolff et al. [67] used a sampling strategy to study changes in dryland woodlands in Morocco at the tree level, while Song et al. [30] employed sampling to assess forest cover change rates in Sichuan Province, China, over an area of 484,000 km^2.

One possibility to increase the use of CORONA imagery in the research community is to provide access to geometrically corrected imagery. The CORONA Atlas & Referencing System, developed by the University of Arkansas' Center for Advanced Spatial Technologies (CAST) [68], carried out the orthorectification of a subset of CORONA imagery and provided free public access to the georeferenced dataset. The imagery covered mostly the Middle East, and while it was primarily dedicated to archaeological studies [63], it was also used in other domains of science. For instance, Saleem et al. [41] used the CORONA

Atlas to map LULC in the 1960s in northern Iraq for the study area exceeding 40,000 km^2, for which they produced a wall-to-wall LULC map from images available in the CORONA Atlas archive.

We found out that forests were the most frequently studied LULC category. Forests were studied in different climatic zones such as central Poland [28], southern Morocco [67], western Russia [52], Canada [69], southeastern China [30], Norway [39] or Brazil [6], which show that CORONA, due to its appropriate high resolution, was good enough to capture extent and properties of various forest types in diverse environmental settings. Another frequently studied category is built-up areas in urban and peri-urban settings. For example, Shalaby et al. [55] studied the directions of urban expansion and confirmed that the high spatial resolution of declassified images was sufficient to accurately map initial morphologic features. Pan et al. [70] monitored the urban expansion of Xining City in China and confirmed the capability of CORONA and its resolution to quantify urban expansion.

In the analyzed studies, manual interpretation (on-screen vectorization) was a dominant approach used to classify LULC based on CORONA images. Manual interpretation is preferred over automated approaches due to the risk of errors in the latter because of poor quality and the mismatching of trained samples [26]. A minority of studies attempted to use automated classification methods. As already noted, OBIA or textural features of CORONA imagery were the most commonly used, with random forests (RF) and support vector machine (SVM) algorithms commonly implemented in image classification. For instance, Song et al. [30] applied various textural features of CORONA imagery and SVM to assess forest cover in the 1960s in a large-scale study of Sichuan Province, China. They confined the analysis using stratified random sampling based on forest cover and its changes occurring since the 1970s, which were assessed using Landsat data. Song et al. [6] used a similar approach to study forest cover changes in Eastern United States and Central Brazil. Chen et al. [71] proposed supervised LULC classification using a combination of the textural and spectral features of CORONA and SPOT images to study long-term changes in the wetlands of Taiwan. Deshpande et al. [44] employed convolutional neural networks and RF to receive a land cover map with five categories, and the latter approach also used the textural features of CORONA imagery. Among studies using automated approaches, most studies report land cover classification accuracies exceeding 90%, especially in the case of binary classifications, such as forest–non-forest, or classifications with a low number of land cover classes [6,26,30,52]. In specific cases, accuracies may drop below 90% for some land cover classes. Chen et al., 2020 [71], observed low user accuracy with respect to pond delimitation (below 60%), while Agapiou in 2021 [45] found that the accuracy for some land cover categories, such as vegetated areas and salt lakes, was below 90%, although the overall accuracy of land cover classification reached 94%.

Quite interestingly, while OBIA seems to be well-suited for interpreting very high-resolution CORONA data, it was used in less than 20% of all considered studies, prevailing, however, among studies preferring the automated approach. In addition, for approaches using a combination of automated and manual methods, image segmentation frequently preceded the visual interpretation of segments [72,73]. One of the reasons for not using OBIA for processing CORONA data even more frequently is the need to maintain high geometric accuracy with respect to the segmentation outputs that typically require working with orthoimages, which are quite demanding in the case of CORONA. It was also relatively rare to use additional data, e.g., field measurements or aerial imagery, during that period to overcome the limitations of CORONA imagery interpretation [43,66,74]. For instance, Andersen and Krzywinski [74] studied 19 sites, each containing a minimum of 30 individual trees that were mapped and measured. They interpreted features located in the CORONA image and compared the outputs to trees recorded in the field.

We found that most of the studies utilizing CORONA imagery are multitemporal, providing a comparison of various geospatial data to detect spatial changes in LULC in multitemporal analyses. The low cost and high spatial resolution of CORONA images offer a fairly effective and straightforward solution for studying long-term LULC evolu-

tion, especially in the case of slow and gradual forest cover expansion [64]. Only seven studies assessed LULC and its changes before the operation of CORONA using historical records, archival maps and older aerial imagery. For example, Jabs-Sobocińska et al. [26] studied post-agricultural forest expansion in the Polish Eastern Carpathians in a multitemporal approach from 1944 to 2019 using war-time German aerial photography dated 1944, CORONA and Sentinel-2 imagery. Due to the high visibility of forest edges in images, CORONA was used specifically to map abandoned agricultural lands that transformed later into forests in the region of post-war resettlements and depopulation. The study of Chen et al. [71] on wetlands and water bodies (irrigation ponds) in Taoyuan City, Taiwan, included two periods: 1904–1960s and 1970–2000. For the first period, the authors used the Taiwan Ancient Land Map Digital Archive (TALM) created in 1904 and CORONA imagery acquired in 1969, while for the latter period, CORONA imagery and SPOT-5 were acquired in 2000.

For the majority of multitemporal case studies (49), CORONA imagery remained the earliest dataset used in the time series. In the analyzed studies, CORONA imagery was used alongside a variety of other geospatial data in various combinations. One of the CORONA features enabling the comparison of CORONA imagery to other geospatial data is its high spatial resolution (1.8–7.5 m), although the spatial resolution at the edges of an image could be much lower than in its central part [43]. In various LULC studies carried out with CORONA imagery, the researchers preferred data with a spatial resolution similar to that of CORONA in order to obtain a comparable scale of measurement, the same sample size and identical geometry [75]. Therefore, in LULC change studies, CORONA images were most frequently compared with very high-resolution satellites or aerial imagery. DeWitt et al. [76] used CORONA imagery jointly with very high-resolution remote sensing data, including IKONOS, WorldView-1 and GeoEye-1, to analyze local-scale LULC changes. Spiekermann et al. [77] used RapidEye imagery, offering images with spatial resolutions similar to CORONA (5 m) that are suitable for studying bare land and sparse vegetation and forests, while Racoviteanu et al. [47] used RapidEye and WorldView-2 to study glacier changes in Nepal. It was also common to compare CORONA data with high-resolution imagery, such as various Landsat satellites or Sentinel-2. For instance, Htwe et al. [46] used Landsat 5 and 7 data from 1989 to 2009 to detect LULC changes related to the transformation of farming systems in Myanmar. Saleem et al. [41] used Landsat Multispectral Scanner, Thematic Mapper, Enhanced Thematic Mapper Plus and Landsat Data Continuity Mission imagery in comparison with CORONA imagery to map and quantify long-term LULC changes in northern Iraq.

The variety of geospatial data used in various studies confirms that CORONA is potentially comparable to a range of recently developed datasets and may be a valuable dataset in LULC change detection studies. Various difficulties related to the processing chain, however, require that CORONA imagery is employed in a general framework of qualitative, post-classification comparison methods [78,79], with independent LULC thematic maps derived from various datasets and later compared to each other using simple thematic map overlays.

Several factors ought to be considered when different datasets are combined to study LULC and its changes, including the availability and quality of geospatial data, user experiences and proficiency of the procedures [80]. Although CORONA imagery is widely used by researchers due to the various advantages it offers, there are also several drawbacks reported in the analyzed papers related to data acquisition and data quality that affect the choices of processing methods. The lack of digital metadata is another factor hampering the use of CORONA in effective large-area mapping [67]. It increases the difficulties of georeferencing, frequently referred to as a time-consuming process that requires available ground control points [6,8,26,28–30,44,64]. The automated approach to classifying CORONA imagery likewise has many difficulties with respect to collecting training samples, characteristics of various phenomena, spectral limitations and radiometric distortions of CORONA [6,66]. Overall, variations in the quality and temporal coverage of

the CORONA imagery collection [64], geometric distortions [30,43,62,63,65] and resultant difficulties in mosaicking [62] have caused researchers to reduce the use of these images.

5. Conclusions

In this overview, publications related to CORONA imagery were systematically analyzed. Although our study provides evidence of the increasing usage of CORONA imagery, we note that several drawbacks prevent their wider application, with the most important barriers being a lack of georeferencing and highly variable radiometric quality. These shortcomings compel researchers to either limit the size of the case study area or use various sampling strategies to cover the study area with a sufficient amount of data, thus decreasing the effort dedicated to georeferencing. Moreover, researchers prefer manual interpretation methods, especially for relatively small areas, over automated classification approaches that may result in low accuracy and misclassifications. Nowadays, the potential of CORONA imagery is becoming increasingly known compared to the past. While our focus was on LULC, roughly 40% of studies that used CORONA imagery were dedicated to other fields such as terrain mapping and analysis, frequently focusing on glacier mapping and mass balance assessment, or archaeology, which was focused upon mostly in the Middle East. However, LULC-related studies prevail, and our analysis shows that the outputs of the CORONA program are suitable sources for analyzing LULC globally, encompassing various land cover categories (mostly forests, wetlands and water and built-up areas) and offering high spatial resolution data for the 1960s and the early 1970s. The declassified imagery has particular potential for detecting and analyzing historical forest changes, as forest cover change is a long-term process requiring historical depth offered by data such as CORONA [26,28,30]. From the perspective of LULC change monitoring, the combination of various datasets with different spectral and spatial resolutions with declassified CORONA imagery was found to be useful, providing a reasonable accuracy with respect to LULC change detection. CORONA imagery was mostly compared to high or very high-resolution data (aerial photographs and satellite imagery) and was used primarily to extend LULC time series to the 1960s, especially in areas with poorly accessible aerial imagery with comparable quality.

Author Contributions: Conceptualization, all authors; methodology, data processing and analysis, all authors; writing—original draft preparation, M.S.; writing—review and editing, all authors; visualization and graphics, M.S.; supervision, J.K. and D.K. All authors have read and agreed to the published version of the manuscript.

Funding: This research received no external funding.

Data Availability Statement: All data supporting the findings of this study are available upon request from the first author.

Acknowledgments: Sincere thanks to the anonymous reviewers and members of the editorial team for their comments and contributions.

Conflicts of Interest: The authors declare no conflict of interest.

Appendix A

Table A1. List of 54 papers included in this review.

Papers	Country(ies)	Area sq km	Mapping Extent	Method	LC Classes	Temporal Aspect
[45] Agapiou, A., 2021.	Cyprus	40 *	Wall to wall	Automated	Built-up, bare land and sparse vegetation, forest, wetland and water	Single moment
[29] Andersen, G.L., 2006.	Egypt	10,000 *	Sampling	Manual	Bare land and sparse vegetation	Multi-temporal
[74] Andersen, G.L.; Krzywinski, K., 2007.	Egypt	10,000 *	Sampling	Manual	Bare land and sparse vegetation	Multi-temporal
[81] Ardelean, F. et al., 2020.	Russia	200	Sampling	Manual	Wetland and water	Multi-temporal
[82] Bhambri, R. et al., 2012.	India	4 *	Wall to wall	Manual	Snow and ice, bare land and sparse vegetation	Multi-temporal
[53] Bolch, T. et al., 2022.	Nepal	2000	Wall to wall	Manual	Snow and ice, wetland and water	Multi-temporal
[54] Brandt, M. et al., 2014.	Mali, Senegal	5000 *	Sampling	Manual	Bare land and sparse vegetation, grassland, cropland, forest	Multi-temporal
[72] Brinkmann, K. et al., 2012.	Niger, Nigeria, Mali, Burkina Faso	4200 *	Wall to wall	Both	Built-up, cropland, grassland, wetland and water, forest, bare land and sparse vegetation	Multi-temporal
[71] Chen, Y.-C. et al., 2020.	Taiwan	900	Wall to wall	Automated	Wetland and water, cropland, built-up	Multi-temporal
[37] Chmielewski, S. et al., 2020.	Poland	2 *	Wall to wall	Both	Built-up, forest, grassland, wetland and water, cropland, bare land and sparse vegetation	Multi-temporal
[83] Conesa et al., 2014.	India	20,000 *	Sampling	Manual	Built-up	Multi-temporal
[44] Deshpande, P. et al., 2021.	India	43 *	Sampling	Automated	Bare land and sparse vegetation, cropland, wetland and water, built-up	Single moment
[76] DeWitt, J.D. et al., 2017.	Côte d'Ivoire	90 *	Sampling	Manual	Bare land and sparse vegetation	Multi-temporal
[8] Dittrich, A. et al., 2010.	China	482	Wall to wall	Manual	Built-up, cropland, grassland, wetland and water	Multi-temporal
[5] Fekete, A., 2020.	Peru	6 *	Wall to wall	Manual	Built-up	Multi-temporal
[69] Franklin, S.E. et al., 2005.	Canada	717.9	Wall to wall	Manual	bare land and sparse vegetation, wetland and water, forest, grassland, snow and ice	Multi-temporal

Table A1. *Cont.*

[84] Ganyushkin, D.A. et al., 2018.	Russia, Mongolia, China	2600	Wall to wall	Manual	Snow and ice	Multi-temporal
[66] Gurjar, S.K.; Tare, V., 2019.	India	22,400	Wall to wall	Both	Wetland and water, cropland, grassland, bare land and sparse vegetation, forest, built-up	Multi-temporal
[85] Hamandawana, H. et al., 2005.	Botswana	60,000 *	Wall to wall	Manual	Wetland and water	Multi-temporal
[86] Herrmann, S. M. et al., 2013.	Senegal	26,000	Sampling	Manual	Forest	Multi-temporal
[46] Htwe, T. et al., 2015	Myanmar	2115	Wall to wall	Manual	Forest, bare land and sparse vegetation, cropland, built-up, wetland and water, grassland	Multi-temporal
[26] Jabs-Sobocińska, Z. et al., 2021.	Poland	2212.44	Wall to wall	Automated	Forest, cropland	Multi-temporal
[87] Jelil Niang, A. et al., 2020.	Saudi Arabia	10 *	Wall to wall	Manual	Built-up	Multi-temporal
[58] Klimetzek, D et al., 2021.	Romania	20.40	Wall to wall	Manual	Forest	Multi-temporal
[40] Lasaponara, R., et al., 2017.	Egypt, Iran	Egypt: 42 * Iran: 8 *	Wall to wall	Automated	Built-up, cropland, wetland and water, bare land and sparse vegetation	Multi-temporal
[65] Leempoel, K. et al., 2013.	China	200	Wall to wall	Manual	Wetland and water, cropland, forest	Multi-temporal
[88] Lele, N. et al., 2015.	India	5.4	Wall to wall	Manual	Grassland	Multi-temporal
[89] Łuców, D. et al., 2020.	Russia	5.44	Wall to wall	Both	Wetland and water, built-up, forest, cropland	Multi-temporal
[90] Mal, S. et al., 2019.	India	250 *	Sampling	Manual	Snow and ice, bare land and sparse vegetation	Multi-temporal
[67] Marzolff, I. et al., 2022.	Morocco	10,000 *	Sampling	Manual	Forest	Multi-temporal
[91] Mergili, M.P. et al., 2013.	Tajikistan, Kyrgyzstan, Afghanistan	98,300	Wall to wall	Manual	Wetland and water	Multi-temporal
[64] Mészáros, M. et al., 2014.	Serbia	230	Wall to wall	Manual	Forest	Multi-temporal
[73] Munteanu, C. et al., 2020.	Kazakhstan	60,000	Sampling	Both	Grassland, cropland,	Multi-temporal
[57] Nistor, C. et al., 2021.	Romania	228	Wall to wall	Manual	Built-up, bare land and sparse vegetation, forest, wetland and water, grassland, cropland	Multi-temporal

Table A1. *Cont.*

[42] Nita, M. D. et al., 2018.	Romania	212,000	Wall to wall	Manual	Forest	Single moment
[70] Pan, X. et al., 2021.	China	231 *	Wall to wall	Automated	Built-up	Multi-temporal
[47] Racoviteanu, A.E. et al., 2022.	Nepal	1971	Wall to wall	Manual	Snow and ice, wetland and water	Multi-temporal
[39] Rannow, S., 2013.	Norway	8000	Wall-to-wall and sampling	Manual	Forest	Multi-temporal
[52] Rendenieks, Z. et al., 2020.	Russia, Latvia	22,209	Sampling	Automated	Forest	Multi-temporal
[62] Rigina, O., 2003.	Russia	2880	Wall to wall	Automated	Forest, bare land and sparse vegetation, built-up, wetland and water	Multi-temporal
[41] Saleem, A. et al., 2018.	Iraq	44,957.1	Wall to wall	Automated	Wetland and water, built-up, forest, bare land and sparse vegetation, cropland	Multi-temporal
[43] Saleem, A. et al., 2021.	Iraq, Iran, Syria	2896.3	Sampling	Both	Built-up, cropland, forest, bare land and sparse vegetation	Single moment
[28] Shahbandeh, M. et al., 2022.	Poland	451.81	Wall to wall	Manual	Forest, cropland, grassland	Multi-temporal
[55] Shalaby, H. et al., 2022.	Egypt	300	Wall to wall	Manual	Built-up	Multi-temporal
[63] She, J. et al., 2014.	China	5518	Sampling	Manual	Snow and ice	Multi-temporal
[6] Song, D.-X. et al., 2015.	USA, Brazil	2000	Sampling	Automated	Forest	Multi-temporal
[30] Song, D.-X. et al., 2021.	China	484,000	Sampling	Automated	Forest	Multi-temporal
[77] Spiekermann, R. et al., 2015.	Mali	3600	Wall to wall	Automated	Forest, bare land and sparse vegetation	Multi-temporal
[56] Stăncioiu, P.T. et al., 2021.	Romania	80,000 *	Sampling	Manual	Forest	Multi-temporal
[92] Stokes, C.R. et al., 2006.	Russia, Georgia	3000 *	Sampling	Manual	Snow and ice	Multi-temporal
[61] Stratoulias & Grekousis, 2021.	Bulgaria	1600 *	Wall to wall	Automated	Built-up	Single moment
[93] Tappan, G. Gray, et al., 2000	Senegal	2133.55	Wall to wall	Manual	Bare land and sparse vegetation, wetland and water, forest, grassland, cropland	Multi-temporal
[38] Victorov, A. et al., 2022.	Russia, USA, Canada	>1 mln *	Sampling	Manual	Wetland and water, bare land and sparse vegetation	Multi-temporal
[21] Zhang, Y. et al., 2020.	China	6 *	Wall to wall	Manual	Forest	Multi-temporal

* denotes the study area's size approximated using maps and data published in the study.

References

1. Burnett, M.G. (Ed.) *Hexagon (KH-9) Mapping Camera Program and Evolution*; Center for the Study of National Reconnaissance: Chantilly, VA, USA, 2012.
2. Wheelon, A.D. Corona: The First Reconnaissance Satellites. *Phys. Today* **1997**, *50*, 24–30. [CrossRef]
3. Mihai, B.; Nistor, C.; Toma, L.; Săvulescu, I. High Resolution Landscape Change Analysis with CORONA KH-4B Imagery. A Case Study from Iron Gates Reservoir Area. *Procedia Environ. Sci.* **2016**, *32*, 200–210. [CrossRef]
4. Ur, J.A. CORONA Satellite Imagery and Ancient Near Eastern Landscapes. In *Mapping Archaeological Landscapes from Space*; Springer Briefs in Archaeology; Springer: New York, NY, USA, 2013; pp. 21–31. [CrossRef]
5. Fekete, A. CORONA High-Resolution Satellite and Aerial Imagery for Change Detection Assessment of Natural Hazard Risk and Urban Growth in El Alto/La Paz in Bolivia, Santiago de Chile, Yungay in Peru, Qazvin in Iran, and Mount St. Helens in the USA. *Remote Sens.* **2020**, *12*, 3246. [CrossRef]
6. Song, D.X.; Huang, C.; Sexton, J.O.; Channan, S.; Feng, M.; Townshend, J.R. Use of Landsat and Corona data for mapping forest cover change from the mid-1960s to 2000s: Case studies from the Eastern United States and Central Brazil. *ISPRS J. Photogramm. Remote Sens.* **2015**, *103*, 81–92. [CrossRef]
7. Yenne, B. *The Encyclopedia of U.S. Spacecraft*; Exeter Books (A Bison Book); Simon & Schuster Books: New York, NY, USA, 1985; ISBN 978-0-671-07580-4.
8. Dittrich, A.; Buerkert, A.; Brinkmann, K. Assessment of land use and land cover changes during the last 50 years in oases and surrounding rangelands of Xinjiang, NW China. *J. Agric. Rural Dev. Trop. Subtrop.* **2010**, *111*, 129–142.
9. Corona Program. Available online: http://space.jpl.nasa.gov/msl/Programs/corona.html (accessed on 13 May 2023).
10. Manaugh, G. Zooming-In on Satellite Calibration Targets in the Arizona Desert. *Atlas Obscura* **2014**. Available online: https://www.atlasobscura.com/places/corona-satellite-calibration-targets (accessed on 10 September 2022).
11. The_CORONA_Program. Available online: https://www.nro.gov/History-and-Studies/Center-for-the-Study-of-National-Reconnaissance/The-CORONA-Program/ (accessed on 27 June 2022).
12. *Corona: America's First Satellite Program*; Center for the Study of Intelligence, Central Intelligence Agency: Langley, VA, USA, 1995. Available online: https://books.google.pl/books?hl=en&lr=&id=7AlgLBVWPV0C&oi=fnd&pg=PR11&dq=CORONA+imagery+satellites&ots=CmowzdDFcm&sig=zEAgEqBjDMi0lifsPnooKFIGMpo&redir_esc=y#v=onepage&q=CORONA%imagery%satellites&f=false (accessed on 20 September 2022).
13. *Declassified Intelligence Satellite Photographs Fact Sheet 090-96*; United States Geological Survey: Reston, VA, USA, 1998.
14. *The CORONA Story*; Center for the Study of National Reconnaissance Classics; Center for the Study of National Reconnaissance: Chantilly, VA, USA, 2013.
15. Gheyle, W.; Bourgeois, J.; Goossens, R.; Jacobsen, K. Scan problems in digital CORONA satellite images from USGS archives. *Photogramm. Eng. Remote Sens.* **2011**, *77*, 1257–1264. [CrossRef]
16. Dashora, A.; Lohani, B.; Malik, J.N. A repository of earth resource information—CORONA satellite programme. *Curr. Sci.* **2007**, *92*, 926–932.
17. Dehecq, A.; Gardner, A.S.; Alexandrov, O.; McMichael, S.; Hugonnet, R.; Shean, D.; Marty, M. Automated Processing of Declassified KH-9 Hexagon Satellite Images for Global Elevation Change Analysis Since the 1970s. *Front. Earth Sci.* **2020**, *8*, 566802. [CrossRef]
18. EarthExplorer. Available online: https://earthexplorer.usgs.gov/ (accessed on 7 November 2022).
19. Challis, K.; Priestnall, G.; Gardner, A.; Henderson, J.; O'hara, S. Corona remotely-sensed imagery in dryland archaeology: The Islamic city of al-Raqqa, Syria. *J. Field Archaeol.* **2004**, *29*, 139–153. [CrossRef]
20. Casana, J.; Cothren, J. The CORONA Atlas Project: Orthorectification of CORONA Satellite Imagery and Regional-Scale Archaeological Exploration in the Near East. In *Mapping Archaeological Landscapes from Space*; Springer Briefs in Archaeology; Springer: New York, NY, USA, 2013; pp. 33–43. [CrossRef]
21. Zhang, Y.; Shen, W.; Li, M.; Lv, Y. Integrating Landsat Time Series Observations and Corona Images to Characterize Forest Change Patterns in a Mining Region of Nanjing, Eastern China from 1967 to 2019. *Remote Sens.* **2020**, *12*, 3191. [CrossRef]
22. Iacone, B.; Allington, G.R.H.; Engstrom, R. A Methodology for Georeferencing and Mosaicking Corona Imagery in Semi-Arid Environments. *Remote Sens.* **2022**, *14*, 5395. [CrossRef]
23. Awange, J.; Kiema, J. CORONA Historical De-classified Products. In *Environmental Geoinformatics*; Environmental Science and Engineering Series (ENVSCIENCE); Springer: Cham, Switzerland, 2019; pp. 191–199. [CrossRef]
24. Rizayeva, A.; Nita, M.D.; Radeloff, V.C. Large-area, 1964 land cover classifications of Corona spy satellite imagery for the Caucasus Mountains. *Remote Sens. Environ.* **2023**, *284*, 113343. [CrossRef]
25. Olariu, B.; Vîrghileanu, M.; Mihai, B.A.; Săvulescu, I.; Toma, L.; Săvulescu, M.G. Forest Habitat Fragmentation in Mountain Protected Areas Using Historical Corona KH-9 and Sentinel-2 Satellite Imagery. *Remote Sens.* **2022**, *14*, 2593. [CrossRef]
26. Jabs-Sobocińska, Z.; Affek, A.N.; Ewiak, I.; Nita, M.D. Mapping mature post-agricultural forests in the polish eastern Carpathians with archival remote sensing data. *Remote Sens.* **2021**, *13*, 2018. [CrossRef]
27. Scollar, I.; Galiatsatos, N.; Mugnier, C. Mapping from CORONA: Geometric Distortion in KH4 Images. *Photogramm. Eng. Remote Sens.* **2016**, *82*, 7–13. [CrossRef]

28. Shahbandeh, M.; Kaim, D.; Kozak, J. The Substantial Increase of Forest Cover in Central Poland Following Extensive Land Abandonment: Szydłowiec County Case Study. *Remote Sens.* **2022**, *14*, 3852. [CrossRef]
29. Andersen, G.L. How to detect desert trees using corona images: Discovering historical ecological data. *J. Arid Environ.* **2006**, *65*, 491–511. [CrossRef]
30. Song, D.-X.; Huang, C.; He, T.; Feng, M.; Li, A.; Li, S.; Pang, Y.; Wu, H.; Mohamed Shariff, A.R.; Townshend, J. Very Rapid Forest Cover Change in Sichuan Province, China: 40 Years of Change Using Images from Declassified Spy Satellites and Landsat. *IEEE J. Sel. Top. Appl. Earth Obs. Remote Sens.* **2021**, *14*, 10964–10976. [CrossRef]
31. Sohn, H.-G.; Kim, G.I.-H.; Yom, J.-H. Mathematical modelling of historical reconnaissance CORONA KH-4B imagery. *Photogramm. Rec.* **2004**, *19*, 51–66. [CrossRef]
32. Ma, L.; Liu, Y.; Zhang, X.; Ye, Y.; Yin, G.; Johnson, B.A. Deep learning in remote sensing applications: A meta-analysis and review. *ISPRS J. Photogramm. Remote Sens.* **2019**, *152*, 166–177. [CrossRef]
33. Page, M.J.; McKenzie, J.E.; Bossuyt, P.M.; Boutron, I.; Hoffmann, T.C.; Mulrow, C.D.; Shamseer, L.; Tetzlaff, J.M.; Akl, E.A.; Brennan, S.E.; et al. The PRISMA 2020 statement: An updated guideline for reporting systematic reviews. *BMJ* **2021**, *372*, n71. [CrossRef] [PubMed]
34. Ghaffarian, S.; Valente, J.; Van Der Voort, M.; Tekinerdogan, B. Effect of attention mechanism in deep learning-based remote sensing image processing: A systematic literature review. *Remote Sens.* **2021**, *13*, 2965. [CrossRef]
35. Gale, M.G.; Cary, G.J.; Van Dijk, A.I.J.M.; Yebra, M. Forest fire fuel through the lens of remote sensing: Review of approaches, challenges and future directions in the remote sensing of biotic determinants of fire behaviour. *Remote Sens. Environ.* **2021**, *255*, 112282. [CrossRef]
36. WorldCover Viewer. Available online: https://viewer.esa-worldcover.org/worldcover/?language=en&bbox=-329.23828124999994,-85.52712796132818,329.23828124999994,85.52712796132818&overlay=false&bgLayer=MapBox_Satellite&date=2022-12-20&layer=WORLDCOVER_2021_MAP (accessed on 20 December 2022).
37. Chmielewski, S.; Bochniak, A.; Natapov, A.; Wezyk, P. Introducing GEOBIA to landscape imageability assessment: A multi-temporal case study of the nature reserve "Kozki", Poland. *Remote Sens.* **2020**, *12*, 2792. [CrossRef]
38. Kudryavtsev, S.; Maslakov, A.; Makarieva, O.; Majorowicz, J.; Victorov, A.; Kapralova, V.; Orlov, T.; Trapeznikova, O.; Arkhipova, M. Research into Cryolithozone Spatial Pattern Changes Based on the Mathematical Morphology of Landscapes. *Energies* **2022**, *15*, 1218. [CrossRef]
39. Rannow, S. Do shifting forest limits in south-west Norway keep up with climate change? *Scand. J. For. Res.* **2013**, *28*, 574–580. [CrossRef]
40. Lasaponara, R.; Murgante, B.; Elfadaly, A.; Qelichi, M.M.; Shahraki, S.Z.; Wafa, O.; Attia, W. Spatial open data for monitoring risks and preserving archaeological areas and landscape: Case studies at Kom el Shoqafa, Egypt and Shush, Iran. *Sustainability* **2017**, *9*, 572. [CrossRef]
41. Saleem, A.; Corner, R.; Awange, J. On the possibility of using CORONA and Landsat data for evaluating and mapping long-term LULC: Case study of Iraqi Kurdistan. *Appl. Geogr.* **2018**, *90*, 145–154. [CrossRef]
42. Nita, M.D.; Munteanu, C.; Gutman, G.; Abrudan, I.V.; Radeloff, V.C. Widespread forest cutting in the aftermath of World War II captured by broad-scale historical Corona spy satellite photography. *Remote Sens. Environ.* **2018**, *204*, 322–332. [CrossRef]
43. Saleem, A.; Awange, J.L.; Corner, R. Exploiting a texture framework and high spatial resolution properties of panchromatic images to generate enhanced multi-layer products: Examples of Pleiades and historical CORONA space photographs. *Int. J. Remote Sens.* **2021**, *42*, 929–963. [CrossRef]
44. Deshpande, P.; Belwalkar, A.; Dikshit, O.; Tripathi, S. Historical land cover classification from CORONA imagery using convolutional neural networks and geometric moments. *Int. J. Remote Sens.* **2021**, *42*, 5144–5171. [CrossRef]
45. Agapiou, A. Land cover mapping from colorized CORONA archived greyscale satellite data and feature extraction classification. *Land* **2021**, *10*, 771. [CrossRef]
46. Htwe, T.N.; Kywe, M.; Buerkert, A.; Brinkmann, K. Transformation processes in farming systems and surrounding areas of Inle Lake, Myanmar, during the last 40 years. *J. Land Use Sci.* **2015**, *10*, 205–223. [CrossRef]
47. Racoviteanu, A.E.; Glasser, N.F.; Robson, B.A.; Harrison, S.; Millan, R.; Kayastha, R.B.; Kayastha, R. Recent Evolution of Glaciers in the Manaslu Region of Nepal from Satellite Imagery and UAV Data (1970–2019). *Front. Earth Sci.* **2022**, *9*, 767317. [CrossRef]
48. Bindschadler, R.; Vornberger, P. Changes in the West Antarctic Ice Sheet since 1963 from declassified satellite photography. *Science* **1998**, *279*, 689–692. [CrossRef]
49. Shahtahmassebi, A.R.; Lin, Y.; Lin, L.; Atkinson, P.M.; Moore, N.; Wang, K.; He, S.; Huang, L.; Wu, J.; Shen, Z.; et al. Reconstructing historical land cover type and complexity by synergistic use of landsat multispectral scanner and CORONA. *Remote Sens.* **2017**, *9*, 682. [CrossRef]
50. Fekete, A.; Priesmeier, P. Cross-border urban change detection and growth assessment for mexican-usa twin cities. *Remote Sens.* **2021**, *13*, 4422. [CrossRef]
51. McDonald, J.K. (Ed.) CIA Cold War Records Series. Available online: https://www.cia.gov/library/center-for-the-study-of-intelligence/csi-publications/books-and-monographs/corona.pdf (accessed on 13 May 2023).
52. Rendenieks, Z.; Nita, M.D.; Nikodemus, O.; Radeloff, V.C. Half a century of forest cover change along the Latvian-Russian border captured by object-based image analysis of Corona and Landsat TM/OLI data. *Remote Sens. Environ.* **2020**, *249*, 112010. [CrossRef]

53. Bolch, T.; Yao, T.; Bhattacharya, A.; Hu, Y.; King, O.; Liu, L.; Pronk, J.B.; Rastner, P.; Zhang, G. Earth Observation to Investigate Occurrence, Characteristics and Changes of Glaciers, Glacial Lakes and Rock Glaciers in the Poiqu River Basin (Central Himalaya). *Remote Sens.* **2022**, *14*, 1927. [CrossRef]
54. Brandt, M.; Romankiewicz, C.; Spiekermann, R.; Samimi, C. Environmental change in time series—An interdisciplinary study in the Sahel of Mali and Senegal. *J. Arid Environ.* **2014**, *105*, 52–63. [CrossRef]
55. Shalaby, H.; Hermas, E.; Khormi, H.; Farghaly, A.M.; ElSayed, A.M.; Alqurashi, A.; Ascoura, I. The Interplay between Spatial Urban Expansion and Morphologic Landscapes East of Cairo, Egypt Using Time Series Satellite Imagery. *ISPRS Int. J. Geo-Inf.* **2022**, *11*, 386. [CrossRef]
56. Stăncioiu, P.T.; Niță, M.D.; Fedorca, M. Capercaillie (*Tetrao urogallus*) habitat in Romania—A landscape perspective revealed by Cold War spy satellite images. *Sci. Total Environ.* **2021**, *781*, 146763. [CrossRef]
57. Nistor, C.; Vîrghileanu, M.; Cârlan, I.; Mihai, B.-A.; Toma, L.; Olariu, B. Remote sensing-based analysis of urban landscape change in the city of bucharest, romania. *Remote Sens.* **2021**, *13*, 2323. [CrossRef]
58. Klimetzek, D.; Stăncioiu, P.T.; Paraschiv, M.; Niță, M.D. Ecological monitoring with spy satellite images—The case of red wood ants in Romania. *Remote Sens.* **2021**, *13*, 520. [CrossRef]
59. Hammer, E.; Ur, J. Near Eastern Landscapes and Declassified U2 Aerial Imagery. *Adv. Archaeol. Pract.* **2019**, *7*, 107–126. [CrossRef]
60. Bilgin, P. A Return to 'Civilisational Geopolitics' in the Mediterranean? Changing Geopolitical Images of the European Union and Turkey in the Post-Cold War Era. *Geopolitics* **2004**, *9*, 269–291. [CrossRef]
61. Stratoulias, D.; Grekousis, G. Information extraction and population estimates of settlements from historic corona satellite imagery in the 1960S. *Sensors* **2021**, *21*, 2423. [CrossRef]
62. Rigina, O. Detection of boreal forest decline with high-resolution panchromatic satellite imagery. *Int. J. Remote Sens.* **2003**, *24*, 1895–1912. [CrossRef]
63. She, J.; Zhang, Y.; Li, X.; Chen, Y. Changes in snow and glacier cover in an arid watershed of the western Kunlun Mountains using multisource remote-sensing data. *Int. J. Remote Sens.* **2014**, *35*, 234–252. [CrossRef]
64. Mészáros, M.; Pavić, D.; Trifunov, S.; Srdanović, M.; Seferovć, S. Possibilities of applying CORONA archive satellite images in forest cover change detection—Example of the Fruška Gora mountain. *Geogr. Pannonica* **2014**, *18*, 96–101. [CrossRef]
65. Leempoel, K.; Satyaranayana, B.; Bourgeois, C.; Zhang, J.; Chen, M.; Wang, J.; Bogaert, J.; Dahdouh-Guebas, F. Dynamics in mangroves assessed by high-resolution and multi-temporal satellite data: A case study in Zhanjiang Mangrove National Nature Reserve (ZMNNR), P.R. China. *Biogeosciences* **2013**, *10*, 5681–5689. [CrossRef]
66. Gurjar, S.K.; Tare, V. Estimating long-term LULC changes in an agriculture-dominated basin using CORONA (1970) and LISS IV (2013–14) satellite images: A case study of Ramganga River, India. *Environ. Monit. Assess.* **2019**, *191*, 217. [CrossRef]
67. Marzolff, I.; Kirchhoff, M.; Stephan, R.; Seeger, M.; Aït Hssaine, A.; Ries, J.B. Monitoring Dryland Trees with Remote Sensing. Part A: Beyond CORONA—Historical HEXAGON Satellite Imagery as a New Data Source for Mapping Open-Canopy Woodlands on the Tree Level. *Front. Environ. Sci.* **2022**, *10*, 896702. [CrossRef]
68. Corona @ CAST UA. Available online: https://corona.cast.uark.edu/ (accessed on 28 December 2022).
69. Franklin, S.E.; Montgomery, P.K.; Stenhouse, G.B. Interpretation of land cover changes using aerial photography and satellite imagery in the Foothills Model Forest of Alberta. *Can. J. Remote Sens.* **2005**, *31*, 304–313. [CrossRef]
70. Pan, X.; Wang, Y.; Liu, Z.; He, C.; Liu, H.; Chen, Z. Understanding urban expansion on the tibetan plateau over the past half century based on remote sensing: The case of Xining city, China. *Remote Sens.* **2021**, *13*, 46. [CrossRef]
71. Chen, Y.-C.; Lin, W.-C.; Hsiao, L.-H.; Cheng, K.-S. A multidecadal change analysis for irrigation ponds in Taoyuan, Taiwan, using multisource data. *Paddy Water Environ.* **2020**, *18*, 1–14. [CrossRef]
72. Brinkmann, K.; Schumacher, J.; Dittrich, A.; Kadaore, I.; Buerkert, A. Analysis of landscape transformation processes in and around four West African cities over the last 50 years. *Landsc. Urban Plan.* **2012**, *105*, 94–105. [CrossRef]
73. Munteanu, C.; Kamp, J.; Nita, M.D.; Klein, N.; Kraemer, B.M.; Müller, D.; Koshkina, A.; Prishchepov, A.V.; Kuemmerle, T. Cold War spy satellite images reveal long-term declines of a philopatric keystone species in response to cropland expansion. *Proc. R. Soc. B Biol. Sci.* **2020**, *287*, 20192897. [CrossRef]
74. Andersen, G.L.; Krzywinski, K. Mortality, recruitment and change of desert tree populations in a hyper-arid environment. *PLoS ONE* **2007**, *2*, e208. [CrossRef]
75. Atkinson, P.M.; Aplin, P. Spatial variation in land cover and choice of spatial resolution for remote sensing. *Int. J. Remote Sens.* **2004**, *25*, 3687–3702. [CrossRef]
76. DeWitt, J.D.; Chirico, P.G.; Bergstresser, S.E.; Warner, T.A. Multi-scale 46-year remote sensing change detection of diamond mining and land cover in a conflict and post-conflict setting. *Remote Sens. Appl. Soc. Environ.* **2017**, *8*, 126–139. [CrossRef]
77. Spiekermann, R.; Brandt, M.; Samimi, C. Woody vegetation and land cover changes in the Sahel of Mali (1967–2011). *Int. J. Appl. Earth Obs. Geoinf.* **2015**, *34*, 113–121. [CrossRef]
78. Tewkesbury, A.P.; Comber, A.J.; Tate, N.J.; Lamb, A.; Fisher, P.F. A critical synthesis of remotely sensed optical image change detection techniques. *Remote Sens. Environ.* **2015**, *160*, 1–14. [CrossRef]
79. Singh, A. Review Article Digital change detection techniques using remotely-sensed data. *Int. J. Remote Sens.* **1989**, *10*, 989–1003. [CrossRef]
80. Rwanga, S.S.; Ndambuki, J.M. Accuracy Assessment of Land Use/Land Cover Classification Using Remote Sensing and GIS. *Int. J. Geosci.* **2017**, *8*, 611–622. [CrossRef]

81. Ardelean, F.; Onaca, A.; Chețan, M.-A.; Dornik, A.; Georgievski, G.; Hagemann, S.; Timofte, F.; Berzescu, O. Assessment of Spatio-Temporal Landscape Changes from VHR Images in Three Different Permafrost Areas in the Western Russian Arctic. *Remote Sens.* **2020**, *12*, 3999. [CrossRef]
82. Bhambri, R.; Bolch, T.; Chaujar, R.K. Frontal Recession of Gangotri Glacier, Garhwal Himalayas, from 1965 to 2006, Measured through Highresolution Remote Sensing Data. *Curr. Sci.* **2012**, *102*, 489–494.
83. Conesa, F.C.; Madella, M.; Galiatsatos, N.; Balbo, A.L.; Rajesh, S.V.; Ajithprasad, P. CORONA Photographs in Monsoonal Semi-Arid Environments: Addressing Archaeological Surveys and Historic Landscape Dynamics over North Gujarat, India. *Archaeol. Prospect.* **2015**, *22*, 75–90. [CrossRef]
84. Ganyushkin, D.A.; Chistyakov, K.V.; Volkov, I.V.; Bantcev, D.V.; Kunaeva, E.P.; Andreeva, T.A.; Terekhov, A.V.; Otgonbayar, D. Present Glaciers of Tavan Bogd Massif in the Altai Mountains, Central Asia, and Their Changes since the Little Ice Age. *Geosci.* **2018**, *8*, 414. [CrossRef]
85. Hamandawana, H.; Eckardt, F.; Chanda, R. Linking Archival and Remotely Sensed Data for Long-Term Environmental Monitoring. *Int. J. Appl. Earth Obs. Geoinf.* **2005**, *7*, 284–298. [CrossRef]
86. Herrmann, S.M.; Wickhorst, A.J.; Marsh, S.E. Estimation of Tree Cover in an Agricultural Parkland of Senegal Using Rule-Based Regression Tree Modeling. *Remote Sens.* **2013**, *5*, 4900–4918. [CrossRef]
87. Jelil Niang, A.; Hermas, E.; Alharbi, O.; Al-Shaery, A. Monitoring Landscape Changes and Spatial Urban Expansion Using Multi-Source Remote Sensing Imagery in Al-Aziziyah Valley, Makkah, KSA. *Egypt. J. Remote Sens. Sp. Sci.* **2020**, *23*, 89–96. [CrossRef]
88. Lele, N.; Singh, C.P.; Singh, R.P.; Chauhan, J.S.; Parihar, J.S. Space-Based Long-Term Observation of Shrinking Grassland Habitat: A Case-Study from Central India. *J. Earth Syst. Sci.* **2015**, *124*, 1389–1398. [CrossRef]
89. Łuców, D.; Lamentowicz, M.; Obremska, M.; Arkhipova, M.; Kittel, P.; Łokas, E.; Mazurkevich, A.; Mróz, T.; Tjallingii, R.; Słowiński, M. Disturbance and Resilience of a Sphagnum Peatland in Western Russia (Western Dvina Lakeland) during the Last 300 Years: A Multiproxy, High-Resolution Study. *Holocene* **2020**, *30*, 1552–1566. [CrossRef]
90. Mal, S.; Mehta, M.; Singh, R.B.; Schickhoff, U.; Bisht, M.P.S. Recession and Morphological Changes of the Debris-Covered Milam Glacier in Gori Ganga Valley, Central Himalaya, India, Derived from Satellite Data. *Front. Environ. Sci.* **2019**, *7*, 42. [CrossRef]
91. Mergili, M.; Müller, J.P.; Schneider, J.F. Spatio-Temporal Development of High-Mountain Lakes in the Headwaters of the Amu Darya River (Central Asia). *Glob. Planet. Change* **2013**, *107*, 13–24. [CrossRef]
92. Stokes, C.R.; Gurney, S.D.; Shahgedanova, M.; Popovnin, V. Late-20th-Century Changes in Glacier Extent in the Caucasus Mountains, Russia/Georgia. *J. Glaciol.* **2006**, *52*, 99–109. [CrossRef]
93. Tappan, G.G.; Hadj, A.; Wood, E.C.; Lietzow, R.W. Use of Argon, Corona, and Landsat Imagery to Assess 30 Years of Land Resource Changes in West-Central Senegal. *Photogramm. Eng. Remote Sens.* **2000**, *66*, 727–735.